Composites Part B 299 (2025) 112390

Contents lists available at ScienceDirect

Composites Part B

journal homepage: www.elsevier.com/locate/compositesb

Low dielectric and high thermal conductivity polyimide nanocomposites with fully closed-loop recycling and highly consistent healing

Zhiyuan Peng, Ling Zhang *, Chunzhong Li **

Key Laboratory for Ultrafine Materials of Ministry of Education, Shanghai Engineering Research Center of Hierarchical Nanomaterials, Frontiers Science Center for Materiobiology and Dynamic Chemistry, School of Materials Science and Engineering, East China University of Science and Technology, Shanghai, 200237, PR China

ARTICLE INFO

Handling Editor: Dr Uday Vaidya

Keywords:
Polyimide nanocomposites
Closed-loop recycling
Efficient healing
Multifunctional materials
Supramolecular chemistry

ABSTRACT

Multifunctional Polyimide (PI) with low dielectric and high thermal conductivity are widely utilized in high-signal-frequency and high-integration electronic devices, yet they are vulnerable to damage within complex operating environments. The development of such high-performance multifunctional composites with recyclable and repairable capability has represented significant challenges. Herein, novelty supramolecular PI nanocomposites comprising Schiff base bonds and hydron bonding interactions via amino-terminated polyimide, functionalized boron nitride nanosheets and aldehyde-containing crosslinking agents maintain the inherent high thermal stability and tensile strength of conventional PI and demonstrate fully closed-loop pH-adjusted liquid-level and high-purity powder-level recyclability, as well as superior healing ability after various mechanical or electrical damage. The resultant PI nanocomposite exhibits notable comprehensive performance, with high recycled in-plane and through-plane thermal conductivity of 8.69 and 5.44 W m^{-1} K^{-1}, low recycled dielectric constant of 2.98 at 1 MHz and excellent healed dielectric breakdown strength of 378.9 kV mm^{-1}, as well as high recovery rates. Furthermore, the repairable triboelectric nanogenerator based on the PI nanocomposite exhibits excellent shape tailorability and nearly-consistent output electrical performance. The concepts presented in this paper offer practical solutions for sustainable high-performance electronic materials and shed light on the integrated structural design of green nanocomposites.

1. Introduction

Nowadays, polymer-based electronic materials are making a splash in emerging fields of integrated circuits (ICs) such as stretchable transistors, electronic skin and brain-computer interfaces [1–4], among which polyimide (PI) stands out among the modern IC materials due to its ability to meet the basic process requirements for microelectronic multilayer circuits [5] with high-temperature stability, excellent corrosion resistance, large-area fabrication capability and special photolithography characteristics [6,7]. However, with the rapid development of high-frequency ICs and high-power electronic devices, there is an urgent need for a multifunctional PI with low dielectric and high thermal conductivity to achieve stable signal transmission and efficient heat dissipation [8]. Moreover, polymer-based electronic devices are susceptible to mechanical and electrical damage under the effect of multi-physical field coupling in complex application environments, resulting in performance degradation or even failure, such as chip interface materials under continuous thermal cycles, thin film transistors (TFT) that are repeatedly folded, and triboelectric nanogenerators (TENG) that are frequently separated from contact [9]. Unfortunately, most PIs, especially thermoset PIs, retain their permanent shape upon curing and are therefore unable to be healed or recycled at all [10]. The non-repairability and non-recyclability of PI have resulted in a significant amount of waste electrical and electronic equipment (WEEE) and loss of raw materials [11,12]. Therefore, the preparation of functional and sustainable PI can both extend the service life of high-performance electronic devices and reduce pollution to protect the environment and human health, which is of great significance for modern green electronics.

The green economy and sustainable development are placing new demands on PI electronic materials for decomposition recycling and restorative healing. While some recyclable or healing designs of PI materials have been reported, they often come at the cost of losing PI's original comprehensive properties [13–19]. Susa et al. [15] synthesized

* Corresponding author.
** Corresponding author.
E-mail addresses: zlingzi@ecust.edu.cn (L. Zhang), czli@ecust.edu.cn (C. Li).

https://doi.org/10.1016/j.compositesb.2025.112390
Received 15 October 2024; Received in revised form 28 December 2024; Accepted 8 March 2025
Available online 17 March 2025
1359-8368/

Composites Part B 299 (2025) 112390

Contents lists available at ScienceDirect

Composites Part B

journal homepage: www.elsevier.com/locate/compositesb

Low dielectric and high thermal conductivity polyimide nanocomposites with fully closed-loop recycling and highly consistent healing

Zhiyuan Peng, Ling Zhang *, Chunzhong Li **

Key Laboratory for Ultrafine Materials of Ministry of Education, Shanghai Engineering Research Center of Hierarchical Nanomaterials, Frontiers Science Center for Materiobiology and Dynamic Chemistry, School of Materials Science and Engineering, East China University of Science and Technology, Shanghai, 200237, PR China

ARTICLE INFO

Handling Editor: Dr Uday Vaidya

Keywords:
Polyimide nanocomposites
Closed-loop recycling
Efficient healing
Multifunctional materials
Supramolecular chemistry

ABSTRACT

Multifunctional Polyimide (PI) with low dielectric and high thermal conductivity are widely utilized in high-signal-frequency and high-integration electronic devices, yet they are vulnerable to damage within complex operating environments. The development of such high-performance multifunctional composites with recyclable and repairable capability has represented significant challenges. Herein, novelty supramolecular PI nanocomposites comprising Schiff base bonds and hydron bonding interactions via amino-terminated polyimide, functionalized boron nitride nanosheets and aldehyde-containing crosslinking agents maintain the inherent high thermal stability and tensile strength of conventional PI and demonstrate fully closed-loop pH-adjusted liquid-level and high-purity powder-level recyclability, as well as superior healing ability after various mechanical or electrical damage. The resultant PI nanocomposite exhibits notable comprehensive performance, with high recycled in-plane and through-plane thermal conductivity of 8.69 and 5.44 W m^{-1} K^{-1}, low recycled dielectric constant of 2.98 at 1 MHz and excellent healed dielectric breakdown strength of 378.9 kV mm^{-1}, as well as high recovery rates. Furthermore, the repairable triboelectric nanogenerator based on the PI nanocomposite exhibits excellent shape tailorability and nearly-consistent output electrical performance. The concepts presented in this paper offer practical solutions for sustainable high-performance electronic materials and shed light on the integrated structural design of green nanocomposites.

1. Introduction

Nowadays, polymer-based electronic materials are making a splash in emerging fields of integrated circuits (ICs) such as stretchable transistors, electronic skin and brain-computer interfaces [1–4], among which polyimide (PI) stands out among the modern IC materials due to its ability to meet the basic process requirements for microelectronic multilayer circuits [5] with high-temperature stability, excellent corrosion resistance, large-area fabrication capability and special photolithography characteristics [6,7]. However, with the rapid development of high-frequency ICs and high-power electronic devices, there is an urgent need for a multifunctional PI with low dielectric and high thermal conductivity to achieve stable signal transmission and efficient heat dissipation [8]. Moreover, polymer-based electronic devices are susceptible to mechanical and electrical damage under the effect of multi-physical field coupling in complex application environments, resulting in performance degradation or even failure, such as chip interface materials under continuous thermal cycles, thin film transistors (TFT) that are repeatedly folded, and triboelectric nanogenerators (TENG) that are frequently separated from contact [9]. Unfortunately, most PIs, especially thermoset PIs, retain their permanent shape upon curing and are therefore unable to be healed or recycled at all [10]. The non-repairability and non-recyclability of PI have resulted in a significant amount of waste electrical and electronic equipment (WEEE) and loss of raw materials [11,12]. Therefore, the preparation of functional and sustainable PI can both extend the service life of high-performance electronic devices and reduce pollution to protect the environment and human health, which is of great significance for modern green electronics.

The green economy and sustainable development are placing new demands on PI electronic materials for decomposition recycling and restorative healing. While some recyclable or healing designs of PI materials have been reported, they often come at the cost of losing PI's original comprehensive properties [13–19]. Susa et al. [15] synthesized

* Corresponding author.
** Corresponding author.
E-mail addresses: zlingzi@ecust.edu.cn (L. Zhang), czli@ecust.edu.cn (C. Li).

https://doi.org/10.1016/j.compositesb.2025.112390
Received 15 October 2024; Received in revised form 28 December 2024; Accepted 8 March 2025
Available online 17 March 2025

an efficient self-healing PI using long aliphatic branched diamine monomers, with the glass transition temperature (T_g) of below 17 °C and a tensile strength of only 6 MPa, which could not meet the dimensional stability of high-temperature circuit preparation and the durability for flexible circuit boards. Guo et al. [19] fabricated the healable and recyclable elastomers composed of rigid PI segments and soft poly (urea-urethane) (PUU) segments with hydrogen bonds. The recycled PI-PUU elastomers exhibited a high tensile strength of 142 MPa and thermal decomposition temperature (T_d) of 320 °C, but the high number of polar groups in PUU significantly increased the dielectric constant and water absorption. Therefore, the preparation of chemically recyclable and repairable PI without affecting its original performance is still a challenging proposition.

In order to develop repairable or healable polymeric materials while retaining as much of their original properties as possible, various dynamic covalent bonds have been designed to achieve chemically reversible reactions or reprocessing [20–22], such as disulfide exchange [23], transesterification reaction [24], Diels-Alder reaction [25] and thiol-Michael chemistry [26]. However, these previously developed materials based on dynamic covalent bonds present certain limitations in terms of the reacquisition of pristine monomers, catalyst dependence and degradation of post-recovery performance [27,28]. Zhang et al. [29] fabricated a recyclable PI via carboxyl ligand exchange between the pendent carboxyl groups and the cyclic Ti-oxo cluster (CTOC) with labile carboxyl ligands. But the surface of CTOC was rich in unstable ligands, which rendered it susceptible to side reactions, affecting the purity of recovered monomers and recovery properties of recycled products.

Contemporarily, there have been several polyimide designs based on dynamic covalent bonding that demonstrate certain recycling or healing capabilities [9,30]. However, these designs focus solely on the polymer component, neglecting the consideration of inorganic fillers. Lyu et al. [31] were only able to incorporate up to 1 wt% of unfunctionalized graphene nanosheets in order to avoid any adverse effects on the healing and recycling properties of vanillin/PI matrix. However, the resulting nanocomposite exhibited a thermal conductivity of only 0.34 W m^{-1} K^{-1}, which falls short of the requirement for efficient heat dissipation during high-load operation. Wu et al. [32] prepared a self-healing poly (urethane-urea-imide) copolymer composited with 40 wt% aluminum nitride and liquid metal fillers with a thermal conductivity of 3.87 W m^{-1} K^{-1}. And the thermal conductivity was reduced by about 10% by reprocessing the material after hot pressing due to the poor interfacial compatibility between the inorganic fillers and matrix. The failure to consider the organic-inorganic composite as a unified entity results in poor overall performance and deterioration of properties following recycling or healing.

In this study, the low dielectric and high thermal conductivity PI nanocomposites with fully closed-loop recycling and efficient healing are prepared by introducing Schiff base dynamic covalent bonds and non-covalent interactions via in-situ polymerization of PI small molecules, functionalized boron nitride nanosheets (BNNS) and crosslinking agents. The resultant supramolecular system exhibits high thermal conductivity (8.69 W m^{-1} K^{-1} for in-plane thermal conductivity) and low dielectric constant (2.98 at 1 MHz) with a performance recovery of 97.6% and 98.7%, respectively, through expedient pH-adjusted liquid-level recycle. Moreover, the powder-level recycle of raw materials with high purity and high yields is achieved through the exploitation of solubility differences. Efficient healing capability has been demonstrated in various types of damage and scales, including dielectric breakdown, corona and mechanical damage through decomposition-repolymerization and hot-pressure-assisted healing, where the dielectric breakdown strength of 378.9 kV mm^{-1} and fractured-healed tensile strength of 51.78 MPa with a performance recovery of 97.9% and 91.0%, respectively. This design provides applicable products for sustainable multi-functional electronic materials in modern electronic devices, as well as integrated design concepts for high-performance green chemistry in line with low-carbon development.

2. Experimental section

2.1. Materials

4,4'-(Hexafluoroisopropylidene)diphthalic anhydride (6FDA, 98%) was supplied by Shanghai Darui Finechem Co., Ltd. (Shanghai, China). 4,4' (Hexafluoroisopropylidene)bis (*p*-phenyleneoxy)dianiline (6FBAPP, 97%) and benzene-1,3,5-tricarboxaldehyde (BTA, 98%) were purchased from Shanghai Macklin Biochemical Co., Ltd. (Shanghai, China). Hexagonal boron nitride (hBN) powder with 3 μm average lateral size was provided from 3M Technical Ceramics (Guangzhou, China). *N*-Methylpyrrolidone (NMP, 99.8%) was received from Shanghai Perfemiker Chemical Technology Co., Ltd. (Shanghai, China). Ethanol (99.7%) was supplied by GENERAL-REAGENT Co. Ltd. (Shanghai, China). Toluene (AR) and hydrochloric acid (HCl, AR) were bought from Sinopharm Chemical Reagent Co., Ltd. (Shanghai, China). All chemicals were used as received without further purification. Deionized water was used throughout the experiment.

2.2. Synthesis of amino terminated polyimide (ATPI)

The polymerization and purification of ATPI prepolymer refer to these literatures [9,30]. The three-necked flask and stirrer were baked with a flame gun 3 times, and the diamine monomer and dianhydride monomer were placed in a vacuum oven at 60 °C overnight. First, 6 mmol of 6FBAPP was dissolved in 30 mL of NMP and stirred for 10 min at room temperature. Then the solution was transferred to an ice-water bath and 3 mmol 6FDA was slowly added under N_2 atmosphere. The precursor solution amino terminated polyamide acid (ATPAA) was formed after stirring for 22 h in a cold bath at 0 °C. Subsequently, 3 mL of toluene was added and heated at 210 °C for 9 h under N_2 atmosphere in a Dean-Stark apparatus. After waiting for cooling, the solution was slowly added dropwise to a vigorously stirred 500 mL ethanol solution followed by the obtaining of a yellowish solid precipitation (ATPI). Finally, ATPI was collected by triple centrifugation and cold ethanol washing. It was dried in an oven at 60 °C for 24 h.

2.3. Preparation of functionalized boron nitride nanosheets (f-BN)

Simultaneously exfoliation and functionalization of hBN was achieved in one step using a high-energy planetary ball milling. Our previous studies have investigated the process parameters of ball milling hBN, including rotational speed, ball milling time, and zirconium beads ratio [33]. In short, hBN (1 g) and 6FBAPP (1 g) were loaded into a 50 mL zirconia tank. The mixture was first rotated on a high-energy planetary ball mill at 500 rpm for 6 h (25 min forward, 25 min reverse and 5 min stop, for a total of 420 min). Then 20 mL of ethanol was added and wet ball milling was continued for 1 h. After ball milling, the mixture was washed with ethanol followed by centrifuging at 1000 rpm for 2.5 min to remove oversized nanosheets. Then, nanosheets were centrifuged 5 times at 11,000 rpm for 10 min with the help of ultrasound to remove the free urea or diamine monomers from the solution. The product was dried in a vacuum oven at 60 °C for 24 h and the dried powder was ground to be ready to use.

2.4. In-situ polymerization of f-BN/PI/BTA nanocomposite films

In a typical procedure, the molar ratio of amine and aldehyde functional groups is maintained at a 1:1 ratio to ensure a high conversion of APTI, f-BN and BTA. A proportion of f-BN (0 g, 0.0437 g or 0.0978 g) was dissolved into 2.8 mL of NMP solution and stirred at 70 °C for 4 h to achieve a well-mixed dispersion. After cooling to room temperature, 0.3612 g of ATPI and 0.03 g of BTA were added to the solution and stirred for 2 h. The mixed solution was quantitatively pipetted onto a glass plate in the oven using a syringe, heated up to 80 °C and held for 30 min. Then increased to 250 °C at a rate of 1 °C min^{-1} and held for 2 h,

resulting in the final 150 μm thickness of PI/BTA, 10 wt% f-BN/PI/BTA and 20 wt% f-BN/PI/BTA, respectively. The overall steps of the experiment are shown in Scheme S1. In addition, 20 wt% hBN/PI/BTA is used as a comparison sample for dielectric constant. The preparation process of 20 wt% hBN/PI/BTA is consistent with 20 wt% f-BN/PI/BTA.

3. Results and discussion

3.1. Design and synthesis of f-bn/PI/BTA systems

In contrast to the conventional preparation of polyimide-based nanocomposites (Fig. 1a), the innovative design of oligomers and reinforcements, along with the integration of organic-inorganic hybrid systems, facilitates a breakthrough in the versatility and performance of recyclable and healable polyimide nanocomposites. As depicted in Fig. 1b, amino-terminated polyimide (ATPI) small molecule prepolymer

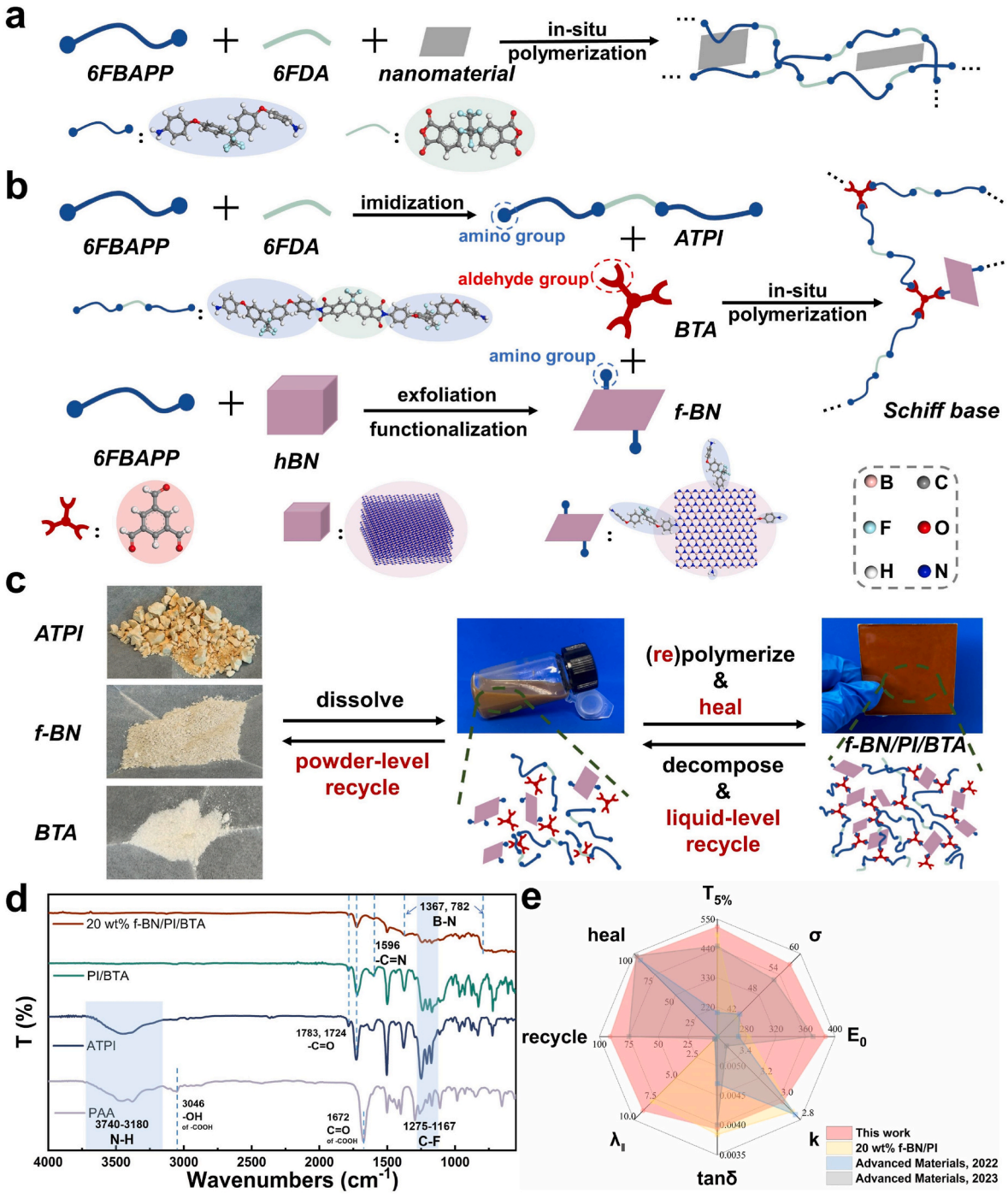

Fig. 1. Schematic illustration of a) conventional PI nanocomposites and b) the molecular composition, reaction process, c) healing and recycling process of f-BN/PI/BTA supramolecular systems with digital photos of ATPI, f-BN, BTA, f-BN/PI/BTA solution and film. d) FTIR of ATPAA, ATPI, PI/BTA and 20 wt% f-BN/PI/BTA. e) A comparison of the fundamental properties of 20 wt% f-BN/PI (this work), 20 wt% f-BN/PI/BTA, HTPI/80 °C (Advanced Materials, 2022) and DCPI (Advanced Materials, 2023).

is synthesized via open-loop aggregation and thermal imidization of trifluoromethyl-containing diamine 6FBAPP and trifluoromethyl-containing dianhydride 6FDA in *N*-Methylpyrrolidone (NMP) at a molar ratio of 2:1. The Fourier transform infrared spectra (FTIR) in Fig. 1b and ^{1}H proton nuclear magnetic resonance spectroscopy (^{1}H-NMR) in Fig. S1 demonstrate the successful synthesis of ATPI. As previously detailed in our study on molecular dynamics study of low dielectric polyimides, the colossal steric hindrance and stronger electrophilicity of trifluoromethyl substituents in ATPI significantly reduce the intermolecular charge transfer complex (CTC) effects, decreasing the polarization rate and dipole moment per unit volume [34]. Functionalized boron nitride nanosheets (f-BN) are prepared by a mechanochemical exfoliation method of hexagonal boron nitride (hBN) with the same diamine monomer (6FBAPP) as polyimide substrate. Our previous study elucidates that 6FBAPP-modified f-BN features few lattice defects, high aspect ratios and chemical grafting modifications displayed in Fig. S2, significantly enhancing the compatibility with matrix and thermal transfer efficiency at the interface. Density functional theory (DFT) binding energy calculations reveal the successful grafting of amino-containing molecular chain segments onto f-BN (Fig. S2i) [35]. Highly dynamic crosslinked supramolecular structures are formed utilizing the aldehyde-based benzene-1,3,5-tricarboxaldehyde (BTA) as crosslinking agents, in conjunction with amino-capped prepolymers ATPI and amino-containing reinforcing phases f-BN via Schiff base reaction. Following the in-situ polymerization and curing at high temperature, the peaks representing the ATPI amino group and the BTA aldehyde group nearly disappear at 3440 and 1696 cm^{-1}, respectively, and a peak at 1596 cm^{-1} representing –C═N appears in the FTIR spectra of PI/BTA and f-BN/PI/BTA films (Fig. 1d), indicating the thorough reaction of the amino and aldehyde groups to form the imine chemical bonds [30].

The complexation energies of the imidization reactions in solution calculated by DFT indicate the theoretical recycling and healing capabilities of f-BN/PI/BTA supramolecular structure (detailed calculations are presented in the Simulation section and Fig. S3 in Supporting Information). The calculated complexation energy for product PI/BTA is positive ($\Delta E^{298K}_{reaction} = 6.463$ kcal mol^{-1}) at room temperature, indicating that the complex formed is not stable enough compared to the reactant monomers, and the Schiff base reaction can be reversible [36]. Similarly, the amino group of the grafted chain segment of 6FBAPP-modified f-BN is capable of forming the reversible Schiff base reaction with aldehyde-contained BTA ($\Delta E^{298K}_{reaction} = 3.083$ kcal mol^{-1}). These reactions are driven in the positive direction due to the volatilization of product water in high-temperature environments, while the imine bonds can decompose back into the corresponding amino and aldehyde groups in certain acidic aqueous solutions. The breaking and reorganization of chemical bonds alter the topology of the polymer network at the molecular level, resulting in dynamic crosslinked composites with recycling and healing capabilities as illustrated in Fig. 1c.

Taking 20 wt% f-BN/PI/BTA films as an example, the supramolecular system combines excellent low dielectric properties (dielectric constant k = 2.95, dielectric loss tanδ = 0.0077 at 1 MHz) and high thermal conductivity (8.90 W m^{-1} K^{-1} for in-plane thermal conductivity) presented in Figs. S4a and b, which render it a promising candidate for use in high-frequency and high-integrity advanced electronic devices. Meanwhile, the dynamic crosslinked network based on an integrated organic-inorganic design displays remarkable thermal stability ($T_{5\%} = 523$ °C), mechanical properties (tensile strength σ = 57 MPa) and dielectric breakdown strength ($E_0 = 387.1$ kV mm^{-1}) shown in S4c-d, thereby satisfying the preparation process of the circuit boards. It is noteworthy that, based on the Schiff base structure, this nanocomposite exhibits an average powder-level recovery of 91.03% for the component monomers and an average retention of properties after healing of 96.25% (described in detail later). As summarized in Fig. 1e, the organic-inorganic integrated and newly designed supramolecular system 20 wt% f-BN/PI/BTA, in comparison to the conventional 20 wt% f-BN/PI nanocomposite and existing sustainable high-performance polyimide materials (HTPI/80 °C [37] and DCPI [9]), not only introduces superior recyclable and repairable features, but also evinces exemplary comprehensive performance.

3.2. Selective decomposition ability of f-bn/PI/BTA systems

For more extensive application prospects, supramolecular material is required to demonstrate stability in a greater variety of environments, and its recyclable and healable capabilities in turn entail that the material possesses highly efficient decomposition ability in specific circumstances. As demonstrated in Fig. 2a, 20 wt% f-BN/PI/BTA nanocomposites show excellent dimensional stability with imperceptible dissolution and swelling phenomena when immersed in various solutions, including sulfuric acid solution with pH = 2, aqueous sodium hydroxide with pH = 13, pure water, ethanol (EtOH), dimethylacetamide (DMAc), tetrahydrofuran (THF) and acetone (AC) stirring at 500 rpm under ambient temperature for 30 days. The 20 wt% f-BN/PI/BTA system is a highly dense supramolecular complex composed of π-π interactions, hydrogen bonds and dynamic imine bonds illustrated in Fig. 2b, which reduces the entry of organic solvent molecules into the system, providing excellent chemical resistance. Furthermore, the trifluoromethyl functional group present in the ATPI exhibits high hydrophobicity, thereby protecting the imine bond from hydrolysis. As a point of comparison, PI/BTA and 10 wt% f-BN/PI/BTA are completely decomposed in pH = 2 sulfuric acid solution displayed in Fig. S5. The deconvolution analysis of the high-resolution FTIR characteristic peaks of H-bonded C═O (1715 cm^{-1}) and free C═O (1738 cm^{-1}) displayed in Figs. S6a–c reveals that the proportion of H-bonded C═O rises from 57.6% to 70.8% with the increase of f-BN, which proves the enhancement of hydrogen bonding in the 20 wt% f-BN/PI/BTA system [38]. X-ray diffraction (XRD) shown in Fig. S6d confirms that the diffraction peak representing the amorphous peak of 20 wt% f-BN/PI/BTA shifts towards larger angles, suggesting a reduction in the matrix chain spacing. The formation of additional imine bonds and hydrogen bonding interactions restricts the mean square displacement (MSD) of the chain segments within the nanocomposites (Figs. S6e and f). The total energy (valence energy and non-bonding energy) of supramolecular systems, as calculated by molecular dynamics, exhibits a marked increase with rising f-BN content in Fig. 2c. Therefore, the stronger interaction and reduced interchain spacing significantly enhance the solvent resistance of the 20 wt% f-BN/PI/BTA nanocomposite.

The recycling/healing of supramolecular systems is essentially the global/localized decomposition and reformulation of dynamic crosslinked networks, respectively. The degradability of PI/BTA and f-BN/PI/BTA nanocomposites is investigated to determine their ability to decompose efficiently under relatively mild conditions. The residual solid mass of film samples is tested after immersing them in NMP solutions with varying HCl concentrations at room temperature and 60 °C for 30 min, respectively (Fig. 2d), and the time taken for complete decomposition at different temperatures (Fig. 2e). The optimal degradation condition for all PI/BTA films is the NMP solution containing 6 wt % HCl solution (12.27 mol/L HCl aqueous solution) at 60 °C, and 20 wt % f-BN/PI/BTA can be dissolved completely within 26 h. The 20 wt% f-BN/PI/BTA supramolecular system, comprising dynamic covalent bonding and strong non-bonding interactions, endows the material with targeted and selective decomposition capabilities, and also contributes to its versatility and durability in practical applications.

3.3. Recycling process and recyclability of f-bn/PI/BTA films

As presented in Fig. 3a, f-BN/PI/BTA possesses the capabilities of liquid-level recycle and powder-level recycle. The clipped film is immersed in a small glass vial containing 6 wt% HCl/NMP solution stirring at 500 rpm under 60 °C. The dynamic imine bonds in the PI/BTA

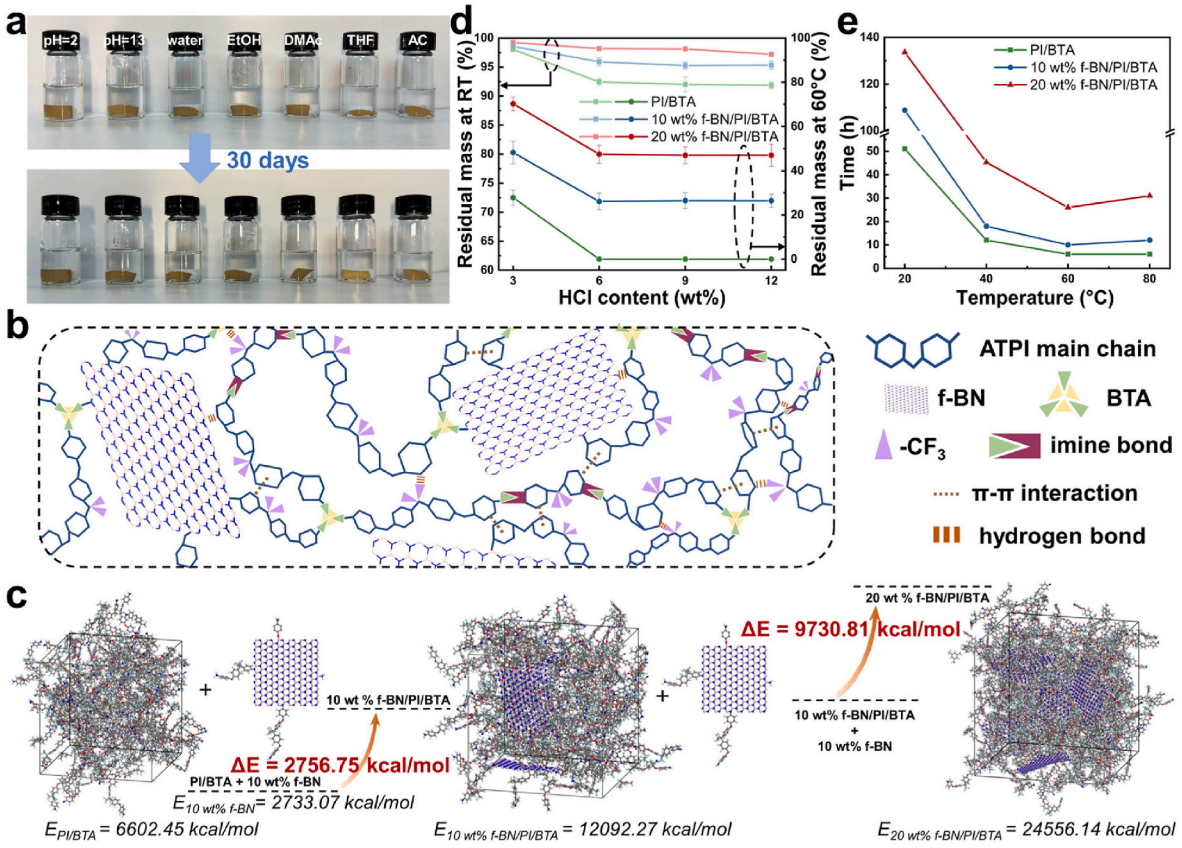

Fig. 2. a) Digital images of 20 wt% f-BN/PI/BTA after immersion in various aqueous solutions and organic solvent at 500 rpm under room temperature for 30 days. b) schematic illustration of the f-BN/PI/BTA nanocomposite structure. c) The total energy change of PI/BTA, 10 wt% f-BN/PI/BTA and 20 wt% f-BN/PI/BTA. d) The residual mass of various PI/BTA samples with different HCl concentrations for 30 min under room temperature and 60 °C. e) The time required for various PI/BTA films (5 cm × 5 cm × 0.15 cm before clipping) to depolymerize complete with 6 wt% HCl concentration stirring at 500 rpm under different temperatures.

and f-BN/PI/BTA films can be dissolved completely in the solution, viz., dissociating solution. When the dissociating solution is poured onto a glass plate and heated to 250 °C for 2 h, the amino functional groups (ATPI and f-BN) and aldehyde functional groups (BTA) can be repolymerized through dynamic covalent bonding, and obtains the recyclable f-BN/PI/BTA or PI/BTA films. The mechanism of liquid-level recycle is illustrated in Fig. 3b. The process of crushing, decomposing, cross-linking and curing of the film is referred to as a cycle of liquid-level recycle. Each cycle can be prepared cyclically using the film repolymerized in the previous cycle. Fig. 3c shows the similar FTIR spectra of the original and 3rd recycled PI/BTA and f-BN/PI/BTA films, including the stretching vibration band of -*C*-N-C (1375 cm^{-1}), the stretching vibration peak representing –C═N (1595 cm^{-1}), and the symmetric and asymmetric vibrations of –C═O (1723 and 1784 cm^{-1}, respectively), which demonstrates the films retain their chemical structure after recycling. The thermal stability of f-BN/PI/BTA exhibited a notable decline, from 522 °C to 473 °C (Fig. 3d) after three liquid-level recycles. Concurrently, the 20 wt% f-BN/PI/BTA film achieves a tensile strength of 43.46 MPa after the third decomposition and recovery, which corresponds to 73.12% of the original 20 wt% f-BN/PI/BTA film's performance shown in Fig. 3e. As illustrated in Figs. S7–9, the thermal stability and mechanical properties of the f-BN/PI/BTA system exhibit a discernible diminution in comparison to the PI/BTA film without f-BN following the process of liquid-level recycle, which is attributed to the significant agglomeration of f-BN after recycling displayed in Fig. 3f. The stability of f-BN in aqueous dispersions is found to be pH-dependent in Fig. S10, which is essentially contingent upon the interaction between the functionalized group grafted on the nanosheets and the aqueous environment [39]. As the acidity of the aqueous solution increases, the zeta potential of the f-BN dispersions decreases, leading to a conspicuous tendency for agglomeration. Following the complete decomposition of the dissociating solution, the pH can be adjusted through the volatility of HCl to ensure that f-BN is restored to a homogeneous dispersed state. Taking 20 wt% f-BN/PI/BTA as an example, the initial pH of the fully decomposed dissociating solution is 0.45, which can be raised to 5.72 after 10 h of stirring in an open bottle at 80 °C presented in Fig. S11. At this point, the f-BN dispersion exhibits high homogeneity without significant sedimentation within 12 h evidenced in Fig. S12. The cross-section scanning electron microscope (SEM) image of 20 wt% f-BN/PI/BTA after three cycles (Fig. 3g) demonstrates that the nanofillers are distributed in a nearly anisotropic and homogeneous manner following pH-adjusted liquid-level recycle, and that the f-BN dispersion is as even as that observed in the original film (Fig. S13). The pH-adjusted liquid-level recycled 20 wt% f-BN/PI/BTA demonstrates remarkable stability of properties, reaching a $T_{5\%}$ of 512 °C (Fig. 3h) and a mechanical strength of 49.84 MPa (Fig. 3i) after three cycles, which are 98.08% and 87.16% of the initial properties, respectively. The original and recycled 20 wt% f-BN/PI/BTA possess stable dielectric constant (k = 2.94–2.98) in Fig. 3l and dielectric loss (tanδ = 0.0077–0.0083) in Fig. S14a at 1 MHz, which also exhibits lower dielectric constant and dielectric loss than commercial Kapton film commonly used in electronics (k = 3.36, tanδ = 0.0123 at 1 MHz) displayed in Fig. S14b. Also, compared to 20 wt% hBN/PI/BTA (k = 3.34, tanδ = 0.0122 at 1 MHz) shown in Fig. S14c, the f-BN with high aspect ratios and superb compatibility with PI matrix plays an important role in facilitating phonon transport efficiency and ameliorating the interfacial defects, obtaining the 20 wt% f-BN/PI/BTA nanocomposite with both high thermal conductivity and low dielectric properties. Meanwhile, the thermal conductivity and dielectric properties of 20 wt% f-BN/PI/BTA exhibit a high degree of consistency during the process of pH-adjusted

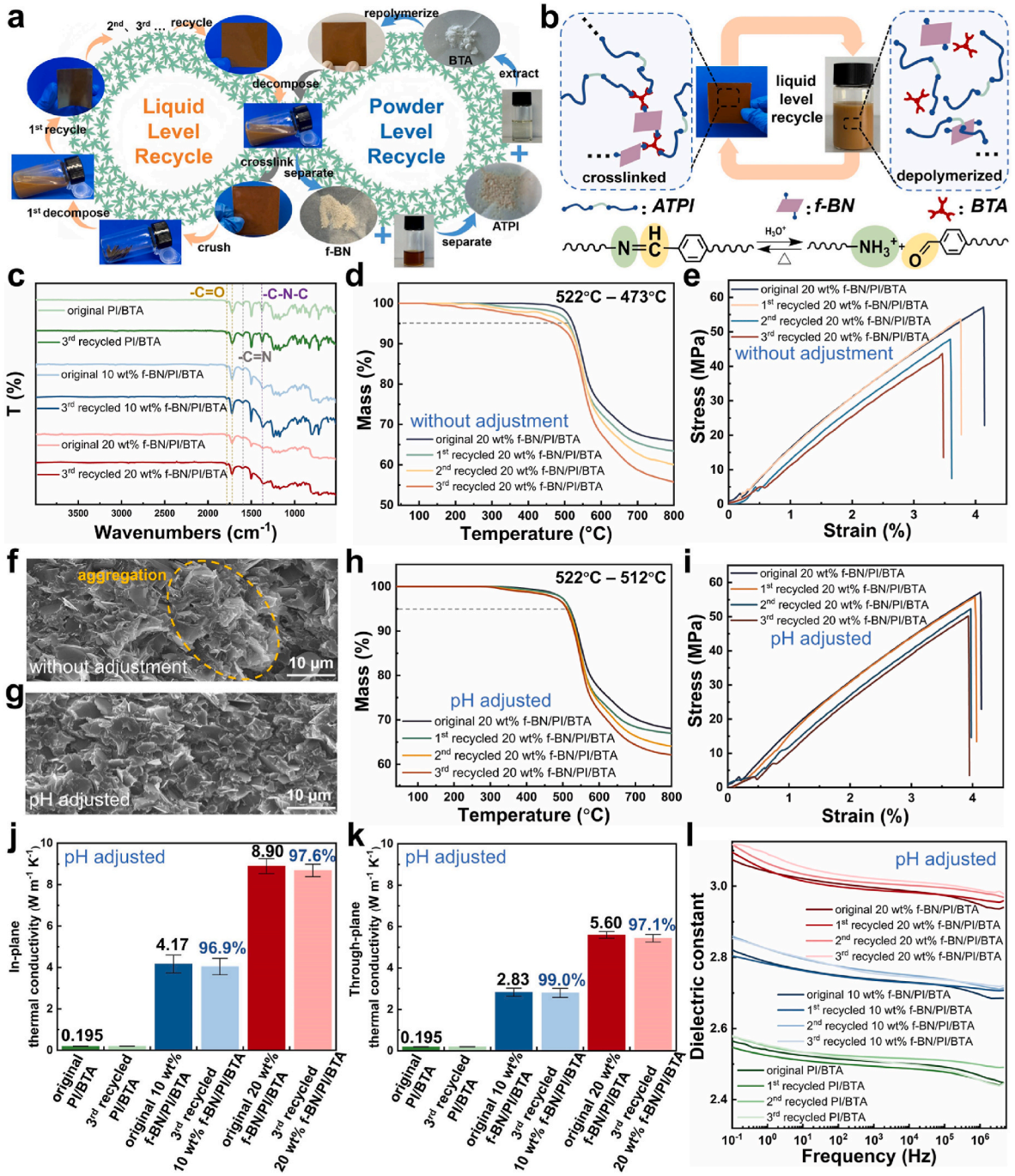

Fig. 3. a) Schematic illustration of the closed-loop liquid-level recycle and powder-level recycle of the 20 wt% f-BN/PI/BTA film. b) Liquid-level recycling of f-BN/PI/BTA based on reversible Schiff base reaction. c) FTIR spectra, d) TGA curves and e) stress-strain patterns of the original and liquid-level recycled 20 wt% f-BN/PI/BTA without pH adjustment. Cross-sectional SEM images of the 20 wt% f-BN/PI/BTA nanocomposite after three liquid-level cycles f) without pH adjustment and g) with pH adjustment. h) TGA curves and i) stress-strain patterns of the original and pH-adjusted liquid-level recycled 20 wt% f-BN/PI/BTA. j) In-plane thermal conductivity, k) through-plane thermal conductivity and l) dielectric constant of the original and pH-adjusted recycled PI/BTA, 10 wt% f-BN/PI/BTA and 20 wt% f-BN/PI/BTA.

liquid-level recycle, demonstrating the potential for reusable functionality.

Selectively recovery of targeted material from mixed polymer wastes or damaged devices is a major challenge, requiring the material with characteristic and efficient recovery properties under mild conditions to separate from other substances [40]. The f-BN/PI/BTA crosslinked network based on dynamic imine bonding has been demonstrated to be efficiently decomposed in 6 wt% HCl solution at 60 °C, and its monomers and fillers can theoretically be further isolated and purified by dissolution, extraction, filtration, evaporation and elution. To substantiate the recyclability of this supramolecular system in the practical application environments, two experiments are conducted illustrated in Fig. 4a: One, the mixed polymer waste contains a variety of plastics, including general plastics (polyethylene (PE), polypropylene (PP), acrylonitrile-butadiene-styrene (ABS)), engineering plastics (polyphenylene ether (PPO), polycarbonate (PC), Kapton polyimide (commercial PI)) and degradable material (polylactic acid (PLA), 20 wt% f-BN/PI/BTA (this work)). Two, the discarded circuit board comprises

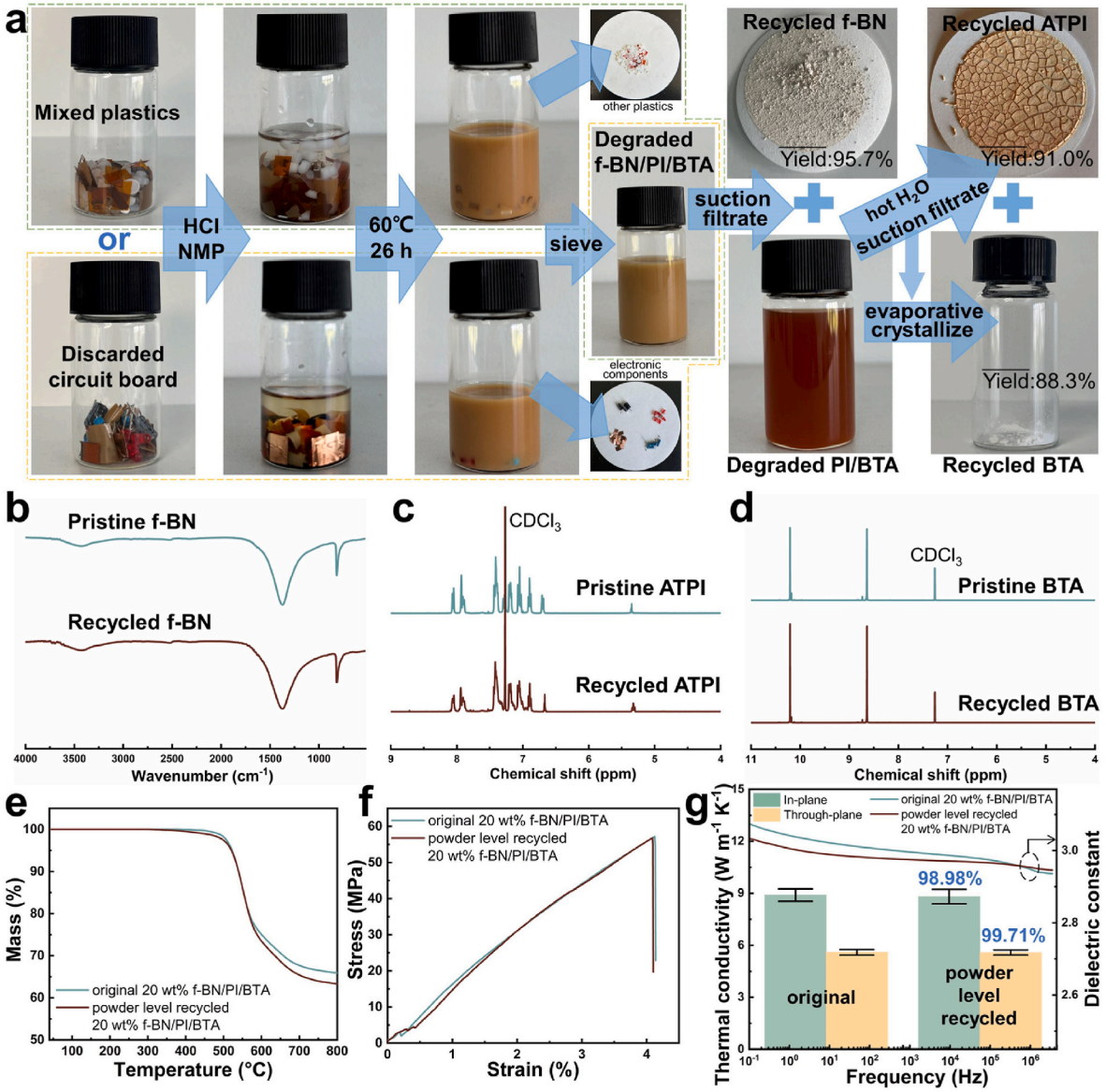

Fig. 4. a) Photographs of the closed-loop recycling of the 20 wt% f-BN/PI/BTA from mixed plastics and discarded circuit board, including the depolymerization of thermoset nanocomposites, the separation of f-BN nanofillers, and the recovery of ATPI and BTA monomers. b) FTIR spectra of pristine and recycled f-BN. ^{1}H-NMR spectra of pristine and recycled c) ATPI and d) BTA. e) TGA curves, f) stress-strain patterns, g) thermal conductivity and dielectric constant of the original and powder-level recycled 20 wt% f-BN/PI/BTA.

wire (copper foil), electronic components (capacitor, resistor, LED) and substrate (20 wt% f-BN/PI/BTA). The chopped materials are dissolved in 10 mL solution of 6 wt% HCl/NMP solution and stirred at 60 °C for 26 h. The 20 wt% f-BN/PI/BTA is selectively depolymerized in this relatively mild acidic solvent, while the other substances would not decompose and dissolve in this environment. The use of a sieve with 1 mm holes allows for the separation of other substances, thereby enabling the retrieval of the degraded f-BN/PI/BTA solution. (The necessary quantity of NMP solution is employed to cleanse the sieve and residues.) To separate the f-BN nanofiller from the solution containing ATPI and BTA monomers, suction filtration is performed using a 0.5 μm filter membrane. Because the rich-aldehyde BTA is easily insoluble in hot water, while amino-terminated ATPI is completely insoluble in hot water, the ATPI would be precipitated by adding excessive hot deionized water into solution. Then, ATPI powder can be further separated by additional suction filtration using a 0.22 μm filter membrane. Eventually, the BTA precipitates out of the mixed solution (HCl/NMP/H_2O) through reduced pressure distillation (water bath temperature of 60 °C and vacuum degree of 80 mbar) and washed with an appropriate amount of *n*-hexane. All separated powders and monomers are treated in a vacuum oven at 80 °C overnight. The average recovery ratios of dried f-BN, ATPI and BTA are calculated at about 95.7%, 91.0% and 88.3%, respectively (Fig. S15). As shown in Fig. 4b–d, the FTIR of the recycled f-BN and ^{1}H NMR of the recovery ATPI and BTA are closely similar to those of the pristine samples. The recycled f-BN possesses similar solution dispersibility, stable chemical structure and excellent interfacial interaction with the matrix as the original f-BN (as shown in Fig. S16). The 20 wt% f-BN/PI/BTA can be prepared again using the recycled powder of monomer and nanofiller, and the material manifests exemplary properties, including thermal stability, mechanical strength, thermal conductivity and low dielectric constant, which remain almost identical to those of the original nanocomposite (Fig. 4e–g). The high yields and high purity of the recovered nanofillers and monomers and the high consistency of properties after powder-level recycle not only demonstrate that f-BN/PI/BTA has the ability of closed-loop powder--level recycle and can be stored in a stable solid phase, but also showcase

the supermolecular system is environmentally friendly and sustainable, with the capability to be separated from mixtures and reprocess for reuse.

3.4. Efficient repairing and healing of f-bn/PI/BTA films

The materials, used as insulating and interlayer dielectric layers in electronic devices, are vulnerable to dielectric breakdown damage and corona damage, and repairing the damaged material is a more economical and convenient method than recycling and reassembly. In contrast to conventional thermosets, Schiff-based PI/BTA and f-BN/PI/BTA materials exhibit efficient healing capability through localized decomposition in dissociating solution and repolymerization during curing. In the case of minor-scale damage, a small amount of dissociating solution is applied and covered with a slide to prevent HCl from evaporating too rapidly. Following an interval at room temperature to permit the complete decomposition of damaged areas, the samples are transferred to an oven and heated to 210 °C for 30 min to repolymerize. As rendered in Fig. S17, PI/BTA displays an excellent capacity to repair the perforation on the surface, as well as the electrical treeing gap within the material resulting from dielectric breakdown. The combination of the large band gap of trifluoromethyl in ATPI [41], and the excellent breakdown resistance and thermal conductivity of BNNS [42,43] enables the f-BN/PI/BTA supramolecular system to mitigate the impact of

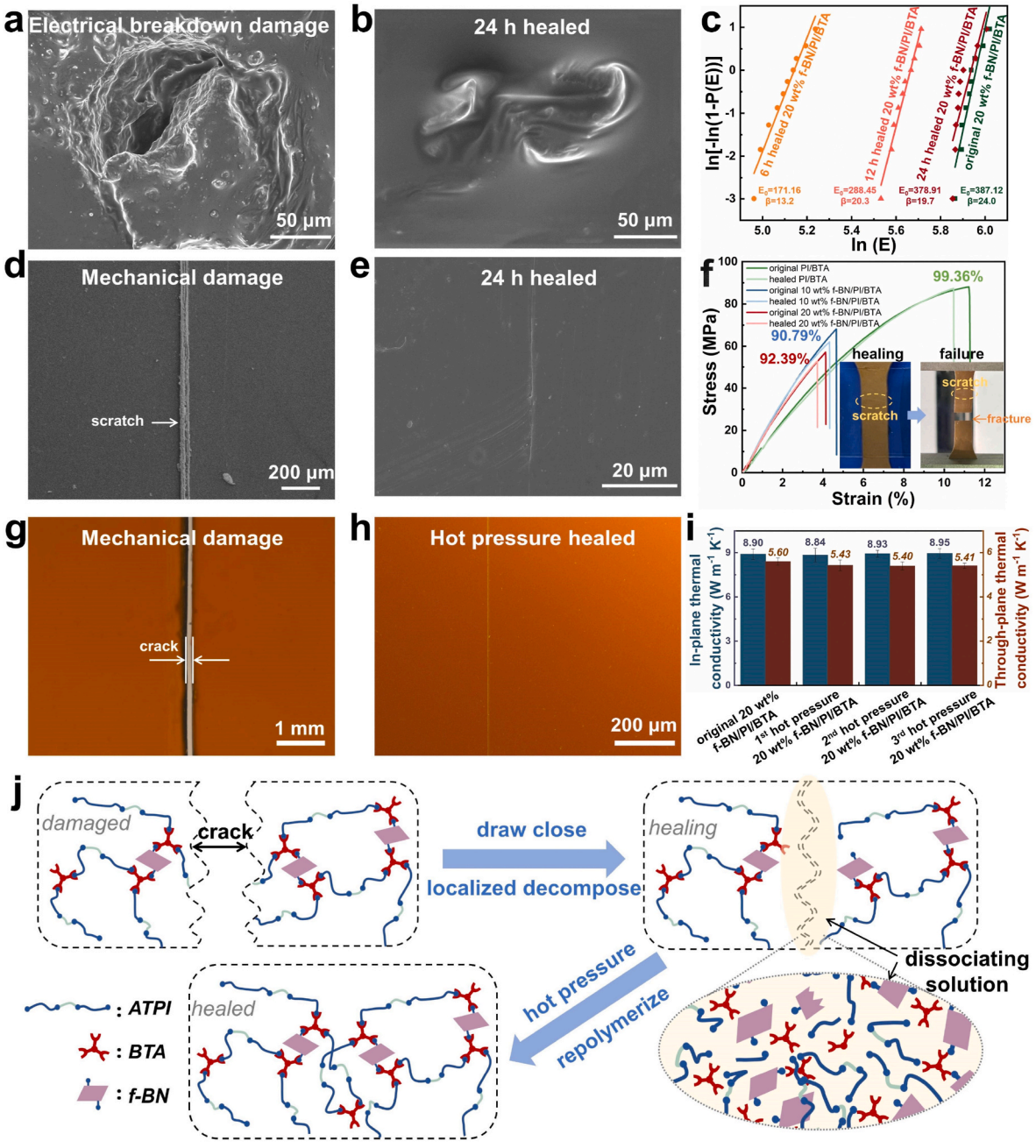

Fig. 5. SEM images of a) dielectric breakdown damage and b) 24-h healed 20 wt% f-BN/PI/BTA. c) Weibull distribution of 20 wt% f-BN/PI/BTA for the original and different healed times after dielectric breakdown damage. SEM images of d) mechanical damage and e) 24-h healed 20 wt% f-BN/PI/BTA. f) Stress-strain curves of the original and 24-h healed PI/BTA and its nanocomposites. Insert: digital photos of the healing process and re-failure sample. Optical images of g) mechanical damage and h) hot-pressure healed 20 wt% f-BN/PI/BTA. i) In-plane and through-plane thermal conductivity of the original and hot-pressure healed 20 wt% f-BN/PI/BTA. j) Schematic illustration of the healing process of the f-BN/PI/BTA film using dissociating solution and welding method.

partial discharge breakdown and thermal breakdown. In addition, the continuous f-BN nanofiller pathway in 20 wt% f-BN/PI/BTA markedly diminishes the local field distortion and impedes the propagation of electrical treeing [44], which significantly leads to a substantial improvement in the dielectric breakdown strength (E_0) of the nanocomposites from 262.1 kV mm^{-1} of PI/BTA to 387.1 kV mm^{-1}. Moreover, the incorporation of f-BN to PI/BTA does not impact the efficacy of healing, where the surface defects can be repaired to a relatively flat topography (Fig. 5a and b). During the healing process, the dissociating solution penetrates into the gaps and is left for varying periods of time, and the thermoset PI/BTA and its nanocomposites exhibit remarkable dielectric breakdown repair ability after 24 h of dissociating decomposition (Fig. S18), in which 20 wt% f-BN/PI/BTA achieves an E_0 of 378.9 kV mm^{-1} and shape parameter (β) of 19.7, with an E_0 recovery rate of 97.88%, as shown in Fig. 5c. Similarly, corona damage can be healed through the process of localized decomposition and repolymerization. The bombardment of the film surface by reactive ions results in the production of carbonized materials and grooves displayed in Fig. S19a and c due to the molecular chain breakage and high-temperature decomposition [9], which can lead to a deterioration of insulating property. Following the removal of the carbonized materials using deionized water, the application of the dissociating solution and the overlaying of a slide allows the materials to regain a smooth and even surface (Figs. S19b and d) and a nearly consistent E_0 demonstrated in Fig. S19e. The 20 wt% f-BN/PI/BTA exhibits an intrinsically high dielectric breakdown strength and demonstrates satisfactory performance recovery from the dielectric breakdown damage and corona damage, which is of great importance for the development of sustainable electrical and electronic materials that can significantly improve the lifetime and operational safety of electrical equipment [45].

Polymer materials are also commonly employed as substrates of flexible circuit boards and encapsulation of electronic devices, which are prone to wear and tear, or even fracture. For minor mechanical injuries, such as slight scratches caused by art knives displayed in Fig. 5d, the healing process of localized decomposition with dissociating solution and repolymerization is highly efficacious (Fig. 5e). The tensile stress-strain curves before and after the scratch repair in Fig. 5f reveal that the mechanical properties of the healed PI/BTA and f-BN/PI/BTA films are largely maintained, with a tensile strength of 52 MPa and an elongation at break of 3.7% for 20 wt% f-BN/PI/BTA. Furthermore, the scratches on the sample are located in the upper part, which becomes inconspicuous after healing, and the fracture location of the repaired sample is not necessarily at the original scratches. However, for the deep scratches, there are still visible internal cracks following the above healing process (Fig. S20) and the completely separated films cannot be healed just through dissociation and repolymerization. Considering high-temperature stress relaxation behavior of dynamic imine bonds, bonding between molecular chains can also be promoted under hot pressure [46,47]. To further assess the comprehensive repair capability of the supramolecular system, especially regarding large-scale mechanical damage, welding method is conducted on the 20 wt% f-BN/PI/BTA films including localized decomposition and hot pressure. The cut samples are positioned as closely as possible along the edge, a small amount of dissociating solution is also dripped into the joints waiting for 2 h, and held under hot pressure at 210 °C with 3.0 MPa pressure for 30 min. As presented in Fig. 5g, h and S21, the completely cut films can be merged into one integrated piece, and the mechanical strength of the 20 wt% f-BN/PI/BTA reaches 51.78 MPa following three cycles of hot-pressure healing, representing a recovery of 91.02% of its original property. The DMA curves of healed 20 wt% f-BN/PI/BTA displayed in Fig. S22 also demonstrate the similar crosslinking degree and chain interactions to the original 20 wt% f-BN/PI/BTA after hot pressure healing. In addition, the thermal conductivity of healed 20 wt% f-BN/PI/BTA exhibits extraordinary retention, almost equal in-plane direction, and a minute decrease in the through-plane direction demonstrated in Fig. 5i. The dissociating solution decomposes some of the imine bonds at the damaged area or fractured edges and fills the voids at the defects or cracks. With the enhanced molecular motion of dynamically imine-bonded polymer at elevated temperatures and the shortening of the molecular chain spacing under high pressures, the reversible dynamic imine bonds begin to undergo rapid chain exchange reactions, and broken hydrogen bonds start to rebuild. Meanwhile, the free ATPI and BTA monomers and f-BN nanofillers in the dissociating solution repolymerize to form the Schiff base structure. The synergistic action facilitates the flattening of irregular areas and accelerates the reconnection of the fractured surfaces into a complete crosslinked network, as depicted in Fig. 5j.

Triboelectric nanogenerators (TENG), as an important component of energy harvesting devices and self-supplied energy sensing systems, demonstrate considerable potential for sustainable energy initiatives and the advancement of the Internet of Things (IoT) [48]. However, TENG is susceptible to material failure due to its operating environment, under the effect of multi-physical field coupling (mechanical friction, heat accumulation, dielectric breakdown, etc) [14]. The incorporation of healable materials into the construction of TENG can significantly prolong their operational lifespan and improve output consistency. The contact-separated TENG consists of a copper foil as the electrode layer and a positive friction layer, a negative friction layer made of 20 wt% f-BN/PI/BTA and a support polyvinyl chloride (PVC) sheet, displayed in Fig. S23. The initial evaluation of TENG output performance is based on a 20 wt% f-BN/PI/BTA with an effective area of 6 × 6 cm^2 and a thickness of approximately 150 μm. Surprisingly, 20 wt% f-BN/PI/BTA-based TENG exhibits satisfactory output performance with open-circuit voltage (V_{OC}) of 78 V, short-circuit current (I_{SC}) of 0.71 μA and short-circuit charge (Q_{SC}) of −36.2 nC, respectively. Compared to a Kapton-based TENG of the same contact area and thickness presented in Figs. S24 and 20 wt% f-BN/PI/BTA-based TENG has an approximate 3-fold performance improvement due to the strong electron-withdrawing effect of the trifluoromethyl groups in 6FDA-6F-BAPP shown in Fig. S25, which increases the charge density and electronegativity [49,50]. As depicted in Fig. 6a, a square of 20 wt% f-BN/PI/BTA film is cut by a cut-off knife into two pieces, and one of the rectangular pieces is then cut into two 3 cm squares. When the negative friction layer of TENG is cut in half, its V_{OC}, I_{SC} and Q_{SC} decrease to about 37 V, 0.33 μA and −17.0 nC, respectively, as shown in Fig. 6b–d. The reason for this is due to the half decrease in the effective contact area which is one of the key factors affecting the output electrical performance of TENG [51]. Then these films are assembled to an area size and smooth surface close to the original film by welding method (the SEM images are shown in Fig. S26). As the two small squares are assembled and healed in turn, their V_{OC}, I_{SC} and Q_{SC} are gradually increased and eventually restored to near-original levels (75 V for V_{OC}, 0.72 μA for I_{SC} and −34.9 nC for Q_{SC}). The excellent self-healing property of imine dynamic covalent bonding enables the 20 wt% f-BN/PI/BTA to recuperate its original shape, allowing the unaltered contact area with positive friction layer. Furthermore, the dielectric constant (Fig. 6e) and dielectric loss (Fig. 6f) of 20 wt% f-BN/PI/BTA film demonstrate stable properties within three hot-pressure healing cycles. Therefore, 20 wt% f-BN/PI/BTA-based TENG still maintains consistent output performance during the three hot-pressure healing cycles. In all, the healed dielectric breakdown, mechanical strength, thermal conductivity and dielectric properties of 20 wt% f-BN/PI/BTA are satisfactory and highly consistent, by the suitable repairing method contingent on the damage types and scales, which is anticipated to be employed as a high-performance electronic material for repairable electronic devices.

4. Conclusion

Polyimide nanocomposites containing Schiff base dynamic covalent bonds are prepared using amino-capped polyimide small molecules, amino-contained-functionalized boron nitride nanosheets and aldehyde-contained crosslinking agents. The synthesized polyimide

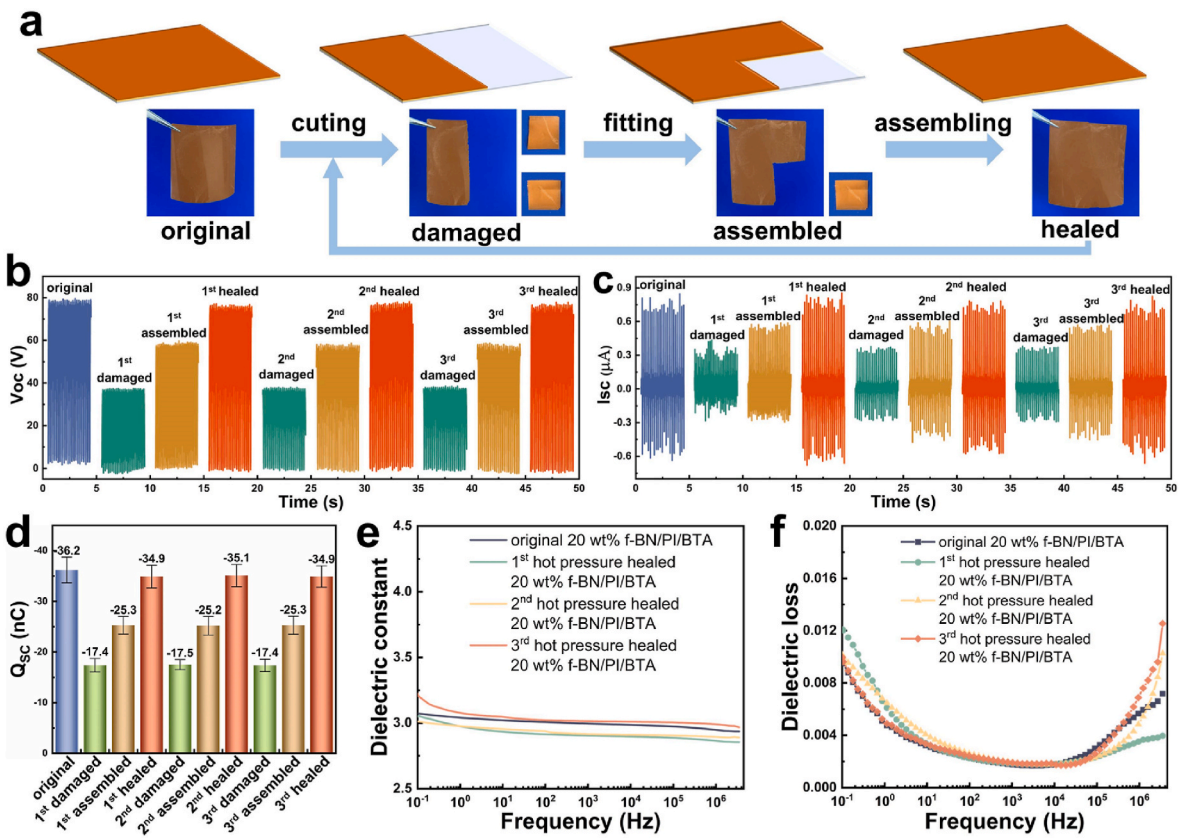

Fig. 6. a) Schematic diagram and digital photos of the healing and assembling process of the 20 wt% f-BN/PI/BTA film. b) Open-circuit voltage, c) short-circuit current and d) short-circuit charge of the 20 wt% f-BN/PI/BTA-based TENG during the healing and assembling process. e) Dielectric constant and f) dielectric loss of the original and hot-pressure healed 20 wt% f-BN/PI/BTA.

nanocomposite, 20 wt% f-BN/PI/BTA, maintains the high thermal stability and high tensile strength of the conventional polyimide nanocomposite (20 wt% f-BN/PI), while also possessing fully closed-loop recyclability and superior healing capability. After three pH-adjusted liquid-level recycles, 20 wt% f-BN/PI/BTA possesses high thermally stable temperature of 512 °C, in-plane and through-plane thermal conductivity of 8.69 and 5.44 W m^{-1} K^{-1}, respectively, and a dielectric constant of 2.98 at 1 MHz. The recovery rates of in-plane and through-plane thermal conductivity are 97.6% and 97.1%, respectively, and the increase in dielectric constant is only 1.3%. Furthermore, the raw materials can be recovered at the powder level by utilizing solubility differences, with yields of 95.7%, 88.3% and 95.7% for PI matrix, BTA crosslinker and f-BN nanofiller, respectively. The 20 wt% f-BN/PI/BTA also demonstrates excellent healing capabilities in mechanical scratches, dielectric breakdown, corona damage and fracture breakage through localized decomposition and welding method, with highly consistent properties. In application, the 20 wt% f-BN/PI/BTA-based TENG exhibits restorable output electrical performance due to its shape and dielectric recoverability through welding method. This strategy of using dynamic covalent bonding of Schiff base in preparing recyclable and repairable multifunctional polyimide material promotes the wider application and sustainable development of high-performance integrated circuit and electronic devices fields.

CRediT authorship contribution statement

Zhiyuan Peng: Writing – original draft, Software, Methodology, Investigation, Formal analysis, Conceptualization. **Ling Zhang:** Writing – review & editing, Supervision, Project administration, Funding acquisition. **Chunzhong Li:** Project administration, Funding acquisition.

Declaration of competing interest

The authors declare that they have no known competing financial interests or personal relationships that could have appeared to influence the work reported in this paper.

Acknowledgements

This work was supported by the National Natural Science Foundation of China (22278140, U22B20143), the Science and Technology Commission of Shanghai Municipality (22DZ1205900). Project was supported by Shanghai Municipal Science and Technology Major Project, the Fundamental Research Funds for the Central Universities.

Appendix B. Supplementary data

Supplementary data to this article can be found online at https://doi.org/10.1016/j.compositesb.2025.112390.

Data availability

Data will be made available on request.

References

[1] Zhong D, Wu C, Jiang Y, Yuan Y, Kim M-g, Nishio Y, et al. High-speed and large-scale intrinsically stretchable integrated circuits. Nature 2024;627(8003):313–20.
[2] Wang W, Jiang Y, Zhong D, Zhang Z, Choudhury S, Lai J-C, et al. Neuromorphic sensorimotor loop embodied by monolithically integrated, low-voltage, soft e-skin. Science 2023;380(6646):735–42.
[3] Tang X, Shen H, Zhao S, Li N, Liu J. Flexible brain–computer interfaces. Nature Electronics 2023;6(2):109–18.

[4] Gong M, Zhang L, Wan P. Polymer nanocomposite meshes for flexible electronic devices. Prog Polym Sci 2020;107:101279.
[5] Liu C, Yu W, Li Y, Wang C, Zhang Z, Li C, et al. Fluorinated polyimide tunneling layer for efficient and stable perovskite photovoltaics. Angew Chem Int Ed 2024: e202402904. n/a(n/a).
[6] Hu R, Chen Y, Zhang C, Jiang S, Hou H, Duan G. Porous monoliths from polyimide: synthesis, modifications and applications. Prog Mater Sci 2024;144:101284.
[7] Parker M. Implantable devices for kidney monitoring. Nature Electronics 2023;6 (10):719.
[8] Li Y, Sun G, Zhou Y, Liu G, Wang J, Han S. Progress in low dielectric polyimide film - a review. Prog Org Coating 2022;172:107103.
[9] Wan B, Xiao M, Dong X, Yang X, Zheng M-S, Dang Z-M, et al. Dynamic covalent adaptable polyimide hybrid dielectric films with superior recyclability. Adv Mater 2023:2304175. n/a(n/a).
[10] Nicholls BT, Fors BP. Closing the loop on thermoset plastic recycling. Science 2024; 384(6692):156–7.
[11] Wang W, Lu X, Li Y, Li X, Sun H, Sun J. Mechanically robust reversibly cross-linked polymers with closed-loop recyclability for use in flexible printed circuit boards. Adv Funct Mater 2024:2401822. n/a(n/a).
[12] Mishra K, Siwal SS, Thakur VK. E-waste recycling and utilization: a review of current technologies and future perspectives. Curr Opin Green Sustainable Chem 2024;47:100900.
[13] Kim YN, Lee J, Kim Y-O, Kim J, Han H, Jung YC. Colorless polyimides with excellent optical transparency and self-healing properties based on multi-exchange dynamic network. Appl Mater Today 2021;25:101226.
[14] Li C, Wang P, Zhang D. Self-healable, stretchable triboelectric nanogenerators based on flexible polyimide for energy harvesting and self-powered sensors. Nano Energy 2023;109:108285.
[15] Susa A, Bose RK, Grande AM, van der Zwaag S, Garcia SJ. Effect of the dianhydride/branched diamine ratio on the architecture and room temperature healing behavior of polyetherimides. ACS Appl Mater Interfaces 2016;8(49): 34068–79.
[16] Zhang X, Li P, Zeng J, Li J, Wang B, Gao W, et al. Dynamic covalent bond enabled strong Bio-based polyimide materials with Thermally-driven Adaptivity, healability and recycling. Chem Eng J 2023;465:143017.
[17] Lee S, Hong PH, Kim J, Choi K, Moon G, Kang J, et al. Highly self-healable polymeric blend synthesized using polymeric glue with outstanding mechanical properties. Macromolecules 2020;53(6):2279–86.
[18] Wan B, Zha J-W. Dynamic polyimide dielectric film: a concept and application perspective. Adv Funct Mater 2024;34(13):2312829.
[19] Guo Z, Lu X, Wang X, Li X, Li J, Sun J. Engineering of chain rigidity and hydrogen bond cross-linking toward ultra-strong, healable, recyclable, and water-resistant elastomers. Adv Mater 2023;35(21):2300286.
[20] Shieh P, Zhang W, Husted KEL, Kristufek SL, Xiong B, Lundberg DJ, et al. Cleavable comonomers enable degradable, recyclable thermoset plastics. Nature 2020;583 (7817):542–7.
[21] Lei Z, Chen H, Luo C, Rong Y, Hu Y, Jin Y, et al. Recyclable and malleable thermosets enabled by activating dormant dynamic linkages. Nat Chem 2022;14 (12):1399–404.
[22] Clarke RW, Sandmeier T, Franklin KA, Reich D, Zhang X, Vengallur N, et al. Dynamic crosslinking compatibilizes immiscible mixed plastics. Nature 2023;616 (7958):731–9.
[23] Zheng Z, Li J, Wei K, Tang N, Li M-H, Hu J. Bioinspired integrated auxetic elastomers constructed by a dual dynamic interfacial healing strategy. Adv Mater 2023;35(42):2304631.
[24] Jang Y-J, Nguyen S, Hillmyer MA. Chemically recyclable linear and branched polyethylenes synthesized from stoichiometrically self-balanced telechelic polyethylenes. J Am Chem Soc 2024;146(7):4771–82.
[25] Wu Y, Chen M, Zhao G, Qi D, Zhang X, Li Y, et al. Recyclable solid–solid phase change materials with superior latent heat via reversible anhydride-alcohol crosslinking for efficient thermal storage. Adv Mater 2024:2311717. n/a(n/a).
[26] Stubbs CJ, Khalfa AL, Chiaradia V, Worch JC, Dove AP. Intrinsically Re-curable photopolymers containing dynamic thiol-michael bonds. J Am Chem Soc 2022;144 (26):11729–35.
[27] Wang S, Feng H, Lim JYC, Li K, Li B, Mah JJQ, et al. Recyclable, malleable, and strong thermosets enabled by knoevenagel adducts. J Am Chem Soc 2024;146(14): 9920–7.
[28] Wang S, Li B, Zheng J, Surat'man NEB, Wu J, Wang N, et al. Nanotechnology in covalent adaptable networks: from nanocomposites to surface patterning. ACS Mater Lett 2023;5(2):608–28.
[29] Zhang G, Chen Q, Xie C, Wang Y, Zhao C, Xiao C, et al. Mechanical-robust and recyclable polyimide substrates coordinated with cyclic Ti-oxo cluster for flexible organic solar cells. Flexible Electronics 2022;6(1):37. npj.
[30] Wan B, Zheng M-S, Yang X, Dong X, Li Y, Mai Y-W, et al. Recyclability and self-healing of dynamic cross-linked polyimide with mechanical/electrical damage. Energy & Environmental Materials 2023;6(1):e12427.
[31] Lyu M, Liu Y, Yang X, Liang D, Wang Y, Liang X, et al. Vanillin-based liquid crystalline polyimine thermosets and their composites for recyclable thermal management application. Compos B Eng 2023;250:110462.
[32] Wu Z, Dong J, Guo H, Shang R, Qin X, Xia Y, et al. Robust, self-healing, and multi-use poly(urethane-urea-imide) elastomer as a durable adhesive for thermal interface materials. Small 2024:2401815. n/a(n/a).
[33] Yang L, Guo J, Zhang L. Superior thermally conductive, mechanically strong and electrically insulating nacre-mimetic chitosan/boron nitride nanosheet composite via evaporation-induced self-assembly method. Polymer 2023;280:126016.
[34] Peng Z, Ye A, Zhang L, Li X, Lian C, Li C. Micro-crosslinked polyimide nanocomposites with low dielectric constant and low dielectric loss for microwave antenna with molecular dynamics. Compos Commun 2024;46:101804.
[35] Peng Z, Guo Q, Zhang L, Li C. High thermal conductivity and low dielectric polyimide nanocomposites using diamine-assisted mechanochemical exfoliation boron nitride and in-situ polymerization under pressure. Chem Eng J 2024;488: 150824.
[36] Acar N, Selçuki C, Coşkun E. DFT and TDDFT investigation of the Schiff base formed by tacrine and saccharin. J Mol Model 2016;23(1):17.
[37] Wan B, Yang X, Dong X, Zheng M-S, Zhao Q, Zhang H, et al. Dynamic sustainable polyimide film combining hardness with softness via a "mimosa-like" bionic strategy. Adv Mater 2023;35(2):2207451.
[38] Li Z, Zhu Y-L, Niu W, Yang X, Jiang Z, Lu Z-Y, et al. Healable and recyclable elastomers with record-high mechanical robustness, unprecedented crack tolerance, and superhigh elastic restorability. Adv Mater 2021;33(27):2101498.
[39] Li Y, Huang T, Chen M, Wu L. Simultaneous exfoliation and functionalization of large-sized boron nitride nanosheets for enhanced thermal conductivity of polymer composite film. Chem Eng J 2022;442:136237.
[40] Lu X, Xie P, Li X, Li T, Sun J. Acid-cleavable aromatic polymers for the fabrication of closed-loop recyclable plastics with high mechanical strength and excellent chemical resistance. Angew Chem Int Ed 2024;63(7):e202316453.
[41] Tao X, Li S, Shi Y, Wang X, Tian J, Liu Z, et al. Triboelectric polymer with high thermal charge stability for harvesting energy from 200 °C flowing air. Adv Funct Mater 2021;31(49):2106082.
[42] Guerra V, Wan C, McNally T. Thermal conductivity of 2D nano-structured boron nitride (BN) and its composites with polymers. Prog Mater Sci 2019;100:170–86.
[43] Roy S, Zhang X, Puthirath AB, Meiyazhagan A, Bhattacharyya S, Rahman MM, et al. Structure, properties and applications of two-dimensional hexagonal boron nitride. Adv Mater 2021;33(44):2101589.
[44] Zhu Y, Zhu Y, Huang X, Chen J, Li Q, He J, et al. High energy density polymer dielectrics interlayered by assembled boron nitride nanosheets. Adv Energy Mater 2019;9(36):1901826.
[45] Chen H, Li L, Zhao W, Zhang X-R, Weng L. Corona resistance mechanism of nano-modified polyimide. Polymers 2022;14(24):5469.
[46] Li M-S, Dong Y-W, Quan M, Jiang W. Stabilization of imines and hemiaminals in water by an endo-functionalized container molecule. Angew Chem Int Ed 2022;61 (35):e202208508.
[47] Wang S, Ma S, Li Q, Yuan W, Wang B, Zhu J. Robust, fire-safe, monomer-recovery, highly malleable thermosets from renewable bioresources. Macromolecules 2018; 51(20):8001–12.
[48] Fu S, Hu C. Achieving ultra-durability and high output performance of triboelectric nanogenerators. Adv Funct Mater 2024;34(9):2308138.
[49] Li Y, Luo Y, Deng H, Shi S, Tian S, Wu H, et al. Advanced dielectric materials for triboelectric nanogenerators: principles, methods and applications. Adv Mater 2024:2314380. n/a(n/a).
[50] Wu J, Wang X, He J, Li Z, Li L. Synthesis of fluorinated polyimide towards a transparent triboelectric nanogenerator applied on screen surface. J Mater Chem A 2021;9(10):6583–90.
[51] Guan Q, Lu X, Chen Y, Zhang H, Zheng Y, Neisiany RE, et al. High-performance liquid crystalline polymer for intrinsic fire-resistant and flexible triboelectric nanogenerators. Adv Mater 2022;34(34):2204543.